Bulletin of the Seismological Society of America

This copy is for distribution only by
the authors of the article and their institutions
in accordance with the Open Access Policy of the
Seismological Society of America.

For more information see the publications section
of the SSA website at www.seismosoc.org

THE SEISMOLOGICAL SOCIETY OF AMERICA
400 Evelyn Ave., Suite 201
Albany, CA 94706-1375
(510) 525-5474; FAX (510) 525-7204
www.seismosoc.org

Bulletin of the Seismological Society of America, Vol. 96, No. 2, pp. 536–552, April 2006, doi: 10.1785/0120040200

Site Response and Attenuation in the Puget Lowland, Washington State

by Thomas L. Pratt and Thomas M. Brocher

Abstract Simple spectral ratio (SSR) and horizontal-to-vertical (H/V) site-response estimates at 47 sites in the Puget Lowland of Washington State document significant attenuation of 1.5- to 20-Hz shear waves within sedimentary basins there. Amplitudes of the horizontal components of shear-wave arrivals from three local earthquakes were used to compute SSRs with respect to the average of two bedrock sites and H/V spectral ratios with respect to the vertical component of the shear-wave arrivals at each site. SSR site-response curves at thick basin sites show peak amplifications of 2 to 6 at frequencies of 3 to 6 Hz, and decreasing spectral amplification with increasing frequency above 6 Hz. SSRs at nonbasin sites show a variety of shapes and larger resonance peaks. We attribute the spectral decay at frequencies above the amplification peak at basin sites to attenuation within the basin strata. Computing the frequency-independent, depth-dependent attenuation factor ($Q_{s,\mathrm{int}}$) from the SSR spectral decay between 2 and 20 Hz gives values of 5 to 40 for shallow sedimentary deposits and about 250 for the deepest sedimentary strata (7 km depth). H/V site responses show less spectral decay than the SSR responses but contain many of the same resonance peaks. We hypothesize that the H/V method yields a flatter response across the frequency spectrum than SSRs because the H/V reference signal (vertical component of the shear-wave arrivals) has undergone a degree of attenuation similar to the horizontal component recordings. Correcting the SSR site responses for attenuation within the basins by removing the spectral decay improves agreement between SSR and H/V estimates.

Introduction

Sedimentary basins often amplify seismic waves, especially at lower frequencies containing the fundamental resonance peak (e.g., Liu and Heaton, 1984; Sánches-Sesma *et al.*, 1988, 1993; Frankel, 1994; Wald and Graves, 1998; Pratt *et al.*, 2003), but thick sedimentary sequences can progressively attenuate seismic waves at higher frequencies (Pratt *et al.*, 2003; Li *et al.*, 2006). These effects were demonstrated in the Puget Lowland of Washington State during the 1999 Seismic Hazard Investigations of Puget Sound (SHIPS) experiment, in which 29 receivers spanned the Seattle sedimentary basin from west to east. Shear-wave arrivals from the *M* 7.6 Chi-Chi, Taiwan, earthquake recorded during the experiment provided the first measurements of seismic wave amplification across the Seattle basin relative to crystalline bedrock sites (Brocher *et al.*, 1999, 2000a; Pratt *et al.*, 2003). Analyses of these weak ground motions showed that the Seattle basin amplifies seismic waves by factors of 12 to 16 at 0.3 to 0.5 Hz, and analyses of local earthquakes and blasts recorded on these same instruments showed that the basin attenuates seismic waves at frequencies above about 7 Hz (Pratt *et al.*, 2003). Amplification of low-frequency waves by the Seattle basin was verified by recordings of the 2001 *M* 6.8 Nisqually and the 2002 *M* 7.9 Denali earthquakes on strong-motion instruments of the Pacific Northwest Seismic Network (Frankel *et al.*, 2003; Barberopoulou *et al.*, 2004). Li *et al.* (2006) used waveform data from the 1999 SHIPS experiment to measure attenuation within the Seattle basin and concluded that attenuation partially or completely counters amplification effects within the basin at higher frequencies.

The 1999 SHIPS results, which were limited to the Seattle sedimentary basin and nearby bedrock sites, raised the question of how other sedimentary basins in the region influence high-frequency seismic waves. To address this question, we analyzed data collected during the 1998 SHIPS experiment, in which 50 three-component seismometers were distributed throughout the Puget Lowland and over the largest sedimentary basins in the region (Fig. 1) (Brocher *et al.*, 1999; Fisher *et al.*, 1999). This three-component receiver array was the first and only such array to have a broad, uniform distribution throughout the Puget Lowland, and it therefore provided an important data set for site-response studies. Unfortunately, only three small, local earthquakes were well recorded during the three-week experiment, so we were limited to examining only the high-frequency (>1.5 Hz) response using these data. We estimated site re-

Figure 1. Map of the Puget Lowland region showing the *P*-wave velocity at 2.5 km depth (Van Wagoner *et al.*, 2002) and the locations of earthquakes and receiver sites used in this study. Thin gray lines are the shorelines of Puget Sound, Lake Washington, and Lake Sammamish. The red lines show the approximate outlines of the Everett, Seattle, Muckleshoot, and Tacoma basins, as defined by the 4.25 km/sec contour on the tomographic image (Johnson *et al.*, 1994, 1996; Pratt *et al.*, 1997; Brocher *et al.*, 2001, Van Wagoner *et al.*, 2002). The thick gray lines are the Seattle fault zone (SF), Tacoma fault zone (TF), and Southern Whidbey Island fault zone (SWIF). The SHIPS 98 receiver sites used in this study are shown as solid dots with the station numbers beside them; red dots denote the two reference stations (6011 and 10032). The earthquakes used in the analysis are shown as focal mechanisms. The inset map shows the Cascadia subduction zone region, with dots showing the distribution of earthquakes recorded by the Pacific Northwest Seismic Network (PNSN).

sponses from this array using both the simple spectral ratio (SSR) and horizontal-to-vertical spectral ratio (H/V) methods. From these data we infer that the seismic-wave amplification in our frequency band is greater in the southern Puget Lowland, estimate attenuation factors in the sedimentary basins, and examine the affect of this attenuation on the shapes of site-response curves.

Geologic Setting and Earthquake Recordings

The 1998 SHIPS experiment was designed primarily to obtain a tomographic image of the upper crust beneath the Puget Lowland of Washington State, in the U.S. Pacific Northwest (Fig. 1). The Lowland is a broad valley between the Olympic Mountains and the Cascade Range that is inhabited by over 3 million people, including those in the cities of Everett, Seattle, Tacoma, and Olympia. Beneath the Lowland, Eocene volcanic basement rocks are folded and faulted into a series of structural uplifts and basins (Pratt *et al.*, 1997). Four major sedimentary basins beneath the Lowland, the Everett, Seattle, Muckleshoot, and Tacoma basins, reach depths of 5 to 9 km (Johnson *et al.*, 1994; Pratt *et al.*, 1997; Brocher *et al.*, 2001; Van Wagoner *et al.*, 2002). Structurally uplifted blocks of basement rocks, including the Seattle uplift, Kingston Arch, and the area around the Southern Whidbey Island fault zone (SWIF), separate these sedimentary basins. Even these uplifted areas, however, have a sedimentary cover up to 2 km thick (Fig. 1) (Johnson *et al.*, 1996; Pratt *et al.*, 1997; Brocher *et al.*, 2001, 2004).

As much as a 1.1-km thickness of unconsolidated, primarily Quaternary deposits underlie the Puget Lowland and form the upper parts of the sedimentary basins (Jones, 1996). The thickness of these unconsolidated deposits approximately correlates with the thickness of older sediments, with the Seattle basin containing the greatest accumulations of all ages. The younger Quaternary deposits are glacial sediments that include those associated with the Late Pleistocene advance of the Vashon ice sheet (Galster and Laprade, 1991; Booth, 1994). Postglacial deposits, lahar deposits, and artificial fill now overlie the glacial deposits in areas of low topography and in parts of the cities.

During the 1998 SHIPS experiment, airgun sources were recorded by an array that included 50 three-component, land seismometers deployed throughout the Puget Lowland (Fig. 1, Table 1) (Fisher *et al.*, 1999; Brocher *et al.*, 1999, 2001). These three-component sites either had 4.5-Hz L-28 or 2-Hz L-22 geophones. At all stations, a Refraction Technology, Inc. (Reftek) data logger recorded 100 samples/sec throughout the three-week duration of the experiment. The 1998 SHIPS recorders were sited to maximize three-dimensional tomography coverage without regard for site-response analysis, but their broad distribution throughout the Puget Lowland caused them to be sited over most of the major geologic structures in the area.

For each of our receiver sites we determined the surface geologic unit, the thickness of the unconsolidated strata, and the depth to basement rocks below the sedimentary strata (Table 1). The surface unit was determined from detailed geologic maps (D. Booth and R. Haugerud, written comm., 2000), and we used the map of Jones (1996) for the thickness of the unconsolidated strata. There is great uncertainty in the maximum thickness of unconsolidated sediments because the available well control in many cases provides only a minimum thickness. To estimate the depth to crystalline bed-

Table 1
Receiver Stations

Site	Sensor	Latitude	Longitude	Elevation (m)	Thickness of Unconsolidated Sediment (m)	Total Sediment Thickness (m)	Surface Geologic Unit*
10004	L28	48.05236	−122.23341	89	472	3200	Qvt
10010	L28	47.95012	−121.88737	139	30	800	Tm
10012	L28	47.87189	−122.29232	165	213	4100	Qvt
10018	L28	47.77521	−122.27981	142	350	5300	Qvt
10023	L28	47.72196	−121.89069	114	91	1000	Qvr
10024	L28	47.65700	−122.40850	93	548	6300	Qva
10026	L28	47.64620	−122.16626	149	488	6000	Qvt
10027	L28	47.74043	−121.97816	79	182	3000	Qvt
10032	L22	47.46592	−121.98399	267	<30	2000	Qvt
10034	L28	47.56334	−122.12078	219	30	4100	Tm
10039	L28	47.45223	−122.28156	148	198	2800	Qvt
10040	L28	47.47111	−122.11353	114	198	3700	Qvr
10053	L28	47.14730	−122.59277	102	610	2900	Qvi
10059	L28	47.03820	−122.38978	143	396	0	Qvr
10060	L28	46.95748	−122.22510	143	46	0	Qv
1011	L28	48.32802	−122.61943	30	183	200	Qvt
1014	L28	48.17365	−122.60353	94	930	2400	Qvt
1017	L28	48.01509	−122.55997	61	243	2800	Qvt
1019	L28	47.92208	−122.41042	41	563	4000	Qvt
2001	L22	47.90831	−122.53122	6	274	4000	Qva
2004	L22	47.81583	−122.53806	41	366	2800	Qvt
2012	L28	47.63114	−122.53383	32	502	6300	Qva
2013	L22	47.61271	−122.60715	96	274	5800	Qvt
3002	L28	47.54794	−122.59029	92	366	1800	Qvr
3006	L22	47.47698	−122.54888	128	335	2500	Qvt
3009	L28	47.39031	−122.56419	91	411	1800	Qva
3012	L22	47.29096	−122.62180	58	503	3600	Qvt
3014	L28	47.22738	−122.60925	99	579	3100	Qvt
4001	L22	47.75100	−122.70327	99	457	3500	Qvt
4003	L22	47.64841	−122.78774	56	183	3700	Qvt
4007	L22	47.55361	−122.97433	136	152	2000	Qvt
5002	L28	47.31109	−122.92594	55	396	4000	Qvt
5003	L28	47.47459	−122.73159	122	152	1900	Qvt
5007	L22	47.24915	−122.82293	72	518	3500	Qvt
5008	L28	47.17546	−122.75692	57	610	3000	Qvt
5009	L22	47.39099	−122.39513	122	411	1900	Qvt
6001	L28	47.90120	−122.67049	158	91	900	Qvt
6004	L28	47.84326	−122.71887	134	122	2000	Qvr
6009	L28	47.73029	−123.12343	377	<30	0	E
6011	L28	47.71146	−122.92585	154	<30	0	E
6012	L28	47.70990	−122.82293	52	121	2400	Qvt
7009	L28	47.23547	−123.20967	76	182	900	Qvt
7010	L28	47.23655	−122.99754	60	366	3200	Qvt
8003	L28	47.10356	−122.73843	33	488	3200	Qvt
8006	L28	46.96839	−122.85793	57	91	1800	Qvo
8009	L28	46.82657	−123.06417	48	30	200	Qvo
8012	L28	46.69334	−123.21161	108	30	1000	O

*Tm, E, O = Tertiary, Eocene, or Oligocene rock; Qva = Quaternary Vashon alluvium (unconsolidated) advance (stiff soil); Qvi = Quaternary Vashon interglacial (stiff soil); Qvt = Quaternary Vashon Till (stiff soil); Qvr = Quaternary Vashon recessional (unconsolidated); Qvo = Quaternary Vashon outwash (unconsolidated).

rock, we used the depth to the 4.5 km/sec contour on an updated version of the tomographic model of Van Wagoner *et al.* (2002) as a proxy for the top of bedrock (R. Crosson, written comm., 2003).

The 1998 SHIPS array recorded 61 local earthquakes and quarry blasts (Brocher *et al.*, 1999), but only three local earthquakes yielded clear compressional (*P*) and shear (*S*) arrivals on a majority of stations (Fig. 2, Table 2). Two of these earthquakes were located near the center of our array, and the third lay to its south (Fig. 1). The three earthquakes providing useful signals had coda magnitudes of 2.1, 2.3, and 2.8 (Table 2). Other earthquakes had magnitudes smaller

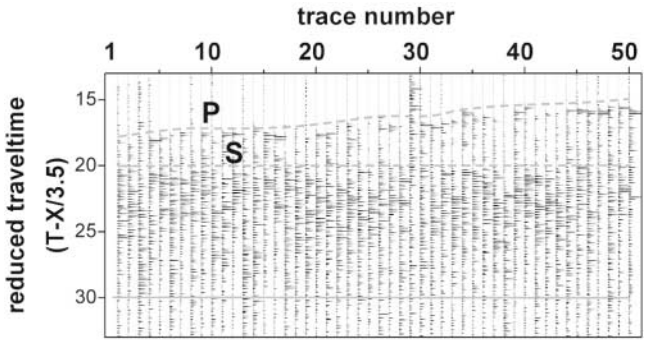

Figure 2. Seismograms of earthquake 18 used in the study, arranged by increasing source–receiver distance, and moved out with a 3.5 km/sec velocity to approximately align the *S*-wave arrivals. The earthquakes were chosen for analysis because they show strong *S*-wave arrivals across the entire array. Dashed gray lines show the arrivals, and the solid gray line shows the end of our 10-sec analysis window.

than 2.0 or were more distant, resulting in weak signals recorded by only limited portions of the array. During the 1998 SHIPS experiment, no arrivals from teleseismic earthquakes were recorded with amplitudes significantly above noise levels.

SSR and H/V Analysis

We computed site responses from shear-wave arrivals using both the SSR and H/V methods. The SSR gives the spectral amplitude ratio between a study site and a bedrock reference site, or the average of several bedrock reference sites. The bedrock site is assumed to record the source spectrum unmodified by site effects, and the SSR therefore measures the influence that the strata below the site of interest have on the spectrum. We used the SSR method instead of a generalized inversion method (Hartzell, 1992), because we had only three events that were recorded at nearly all of the stations, instead of the tens of events normally required for a stable generalized inversion. The two methods have been demonstrated to give nearly identical results (e.g., Field and Jacob, 1995; Dutta *et al.*, 2001; Martirosyan *et al.*, 2002).

The H/V ratio yields the spectral ratio of the horizontal component of the shear-wave arrivals with respect to the vertical component of the same arrivals. The premise of the H/V method is that differences in the shear-wave impedance (velocity times density), which are strongly affected by consolidation, are larger in the shallow deposits than the compressional-wave impedance changes, which are moderated by water saturation. It is assumed the compressional waves are converted from shear waves (*SV* to *P*) at the bedrock surface beneath the shallow deposits and pass largely unaltered through the shallow sediments. The vertical component recording thus serves as a proxy for the shear waves entering the bottom of the shallow deposits and the H/V ratio is believed to measure primarily the influence of the shallow deposits on seismic waves (Lermo and Chávez-García, 1993; Field and Jacob, 1995; Castro *et al.*, 1997; Tsuboi *et al.*, 2001). The H/V ratio is complicated, however, by scattered phases and surface waves propagating within the shallow deposits and contributing to the spectral amplitudes of both the horizontal and vertical components (e.g., Riepl *et al.*, 1998). Because of these complications, and the influence of incidence angle on the percent of mode conversion, the H/V ratio is generally found to show the primary resonance peak but not to accurately determine amplification levels (e.g., Bonilla *et al.*, 1997; Riepl *et al.*, 1998; Parolai and Richwalski, 2004).

Forty-seven sites recorded at least one earthquake well on both horizontal channels (Fig. 1, Table 1). We took the frequency spectrum of each trace in a tapered, 10-sec window starting at the expected *S*-wave arrival. These spectra were corrected for the appropriate instrument response and then smoothed with a tapered, 1.2-Hz running average.

Our analysis is limited to relatively high frequencies of 1.5–20 Hz by our use of small local events. Signal-to-noise levels computed by using a 10-sec noise window before the *P*-wave arrivals show that noise becomes significant below 1.5 Hz (Fig. 3a–h). The 1.5-Hz lower limit excludes the low-frequency (0.3–0.5 Hz) portion of the spectrum where basin amplification is large (Pratt *et al.*, 2003) and where basin surface waves likely are a major factor in amplifying ground shaking (Frankel, 1994; Joyner, 2000; Frankel *et al.*, 2003).

For our SSR reference signal, we averaged the spectra from two bedrock sites on opposite sides of the array to reduce the influence of a single reference site (e.g., Yu and Haines, 2003; Bonilla *et al.*, 1997). The reference sites (6011 and 10032) are located in thin (estimated <5 m) layers of sediment above bedrock near the east and west sides of the array (Fig. 1). Instruments at these sites provided recordings with high signal-to-noise ratios and relatively flat, low-amplitude frequency spectra. For the H/V spectral ratio, we divided the vector sum of the horizontal component spectra at each site by the vertical component spectrum of these same arrivals.

For the SSR method, the spectra were corrected for spherical spreading and attenuation using the standard relation:

$$A_c(f) = A_0(f)\ re^{\pi f t/Q_s(f)}, \tag{1}$$

where $A_c(f)$ = corrected amplitudes, $A_0(f)$ = observed amplitude, r = source-receiver radial distance, f = frequency, t = travel time, and $Q_s(f)$ = the frequency-dependent *S*-wave attenuation factor. Multiplication by the source-receiver distance, r, is consistent with body waves in a uniform medium and with results from attenuation studies in the Cascadia region (Atkinson, 1995). For $Q_s(f)$ we used the bedrock relation of $380f^{0.39}$ derived by Atkinson (1995) and used in previous studies by Frankel *et al.* (1999), Hartzell *et al.* (2000), and Pratt *et al.* (2003). The attenuation correction (equation 1) removed the raw spectra's trend of decreasing

Table 2
Earthquakes Used in the Analysis

Array	Event No.	Date	Origin Time	Latitude	Longitude	Depth (km)	Magnitude
PNSN	6	10-Mar-98	22:03:39	46.50	−122.40	16.9	2.8
SHIPS98	18	17-Mar-98	6:27:58	47.55	−122.37	26.9	2.0
SHIPS98	28	21-Mar-98	22:21:42	47.60	−122.15	13.9	1.6

average spectral amplitude with increasing distance, indicating that the attenuation relation is approximately correct for bedrock in the area. We then computed the SSRs by dividing the vector sum of the horizontal spectra at each site by the reference spectrum computed from the average of the two reference sites. At each receiver site, we independently computed spectral ratios for each earthquake and averaged the responses from the three events to obtain a single SSR. We also plotted one standard deviation above and below the average when the response from more than one earthquake was used (Fig. 3). These estimates of uncertainty suggest that the spectral shapes are generally well constrained even with the limited sample size. To estimate noise levels, we computed the frequency spectra in the noise window and processed them in a manner identical with those containing the signal (dividing by the same SSR reference spectra).

We grouped the individual site-response spectra by geologic setting (see Figs. 1, 3a–h, 5a). To objectively define the deep basin sites, we chose those lying within the 4.25 km/sec contour on the tomography model at 2.5 km depth (Fig. 1). Outside of our basin contours (Figs. 1 and 4), older, more compacted sedimentary rocks lie closer to the surface than at basin sites (e.g., Johnson *et al.*, 1994; Pratt *et al.*, 1997; Brocher *et al.*, 2001, 2004). The thickness of unconsolidated strata also approximately correlates with overall basin thickness, with the thickest unconsolidated deposits (>1100 m) lying over the deepest part of the Seattle basin (Jones, 1996).

In addition to the individual response spectra, we calculated and mapped the average SSR amplification in a broad frequency band (1.5–12.0 Hz) and three one-octave frequency bands: 1.5–3.0 Hz, 3.0–6.0 Hz, and 6.0–12.0 Hz (Fig. 4). These average SSR amplifications are plotted against geologic setting, depth to basement rocks, and surface geologic unit (Fig. 5).

SSR Results

The most striking feature of the SSRs is the similarity in overall shape of site-response curves on the sedimentary basins. All of these basin site responses show peak amplification in the 3- to 6-Hz range. In most cases there is a relatively sharp amplification peak presumably caused by resonance within a prominent shallow layer, although a few sites have broader peaks. The 3- to 6-Hz frequencies correspond to wavelengths of 100–200 m if we assume a shear-wave velocity of 600 m/sec for the Plio-Quaternary alluvium (e.g., Williams *et al.*, 1999, 2000), and these wavelengths imply that the peak resonance occurred in layers about 25 to 50 m thick (1/4 wavelength; e.g., Shearer and Orcutt, 1986). At frequencies above the peak there is a trend of decreasing amplification with higher frequency (Fig. 3a–d). Three of the basin sites show amplification slightly larger than 2 at frequencies near 10 Hz, but otherwise the basin sites have amplifications of 2 or less above 10 Hz and most have amplifications of less than 1. Average amplifications in the 6- to 12-Hz range within the basins are consistently less than 2 (Fig. 5a).

Sites on the Tacoma basin show larger peak amplitudes than those on the basins to the north. Ten of the 13 sites on the Everett basin, Kingston arch, and Seattle basin show peak amplifications of less than 3, but 8 of the 9 Tacoma basin sites show peak amplifications near 3 or greater. On the amplification maps (Fig. 4), relatively uniform, low to moderate amplifications characterize all sites on the Everett and Seattle basins in all frequency ranges. The Tacoma basin sites show the largest amplifications of sites over the deep basins (Figs. 3a–d, 4). The relative amplifications at basin sites are lowest in the 6- to 12-Hz frequency range, consistent with the observed spectral decay at higher frequencies (Figs. 3a–d, 4, 5a).

In contrast to the spectral decay at higher frequencies that characterizes all the deep basin site-response curves, only a bare majority (52%) of the nonbasin sites shows significant spectral decay. About half of the nonbasin sites show either a nearly flat trend (26%) or an increase in amplification with increasing frequency (22%; Fig. 3–h). Nonbasin sites also show the largest resonance peaks in the array. There are large (≥6) resonance peaks at five of the nonbasin sites, whereas none of the basin sites show a peak greater than 6. Four of the nonbasin sites show two or more resonance peaks with amplitudes greater than 4, whereas none of the basin sites have two peaks above 4. About a third of the nonbasin sites show amplifications greater than 2 in the 10- to 20-Hz range.

The differences between deep-basin and nonbasin sites are apparent on plots of amplification versus depth to basement rocks (Fig. 5b). The spectral ratios show a large scatter of amplifications where bedrock is shallow (<2 km), but as bedrock deepens to 7 km the amplifications converge toward a value of near 2 at the low end of our frequency range (1.5–3 Hz) and a value near 1 at higher frequencies (6–12 Hz). The sites with the thickest sedimentary section were located over the Seattle basin, and amplifications of 1 or less for

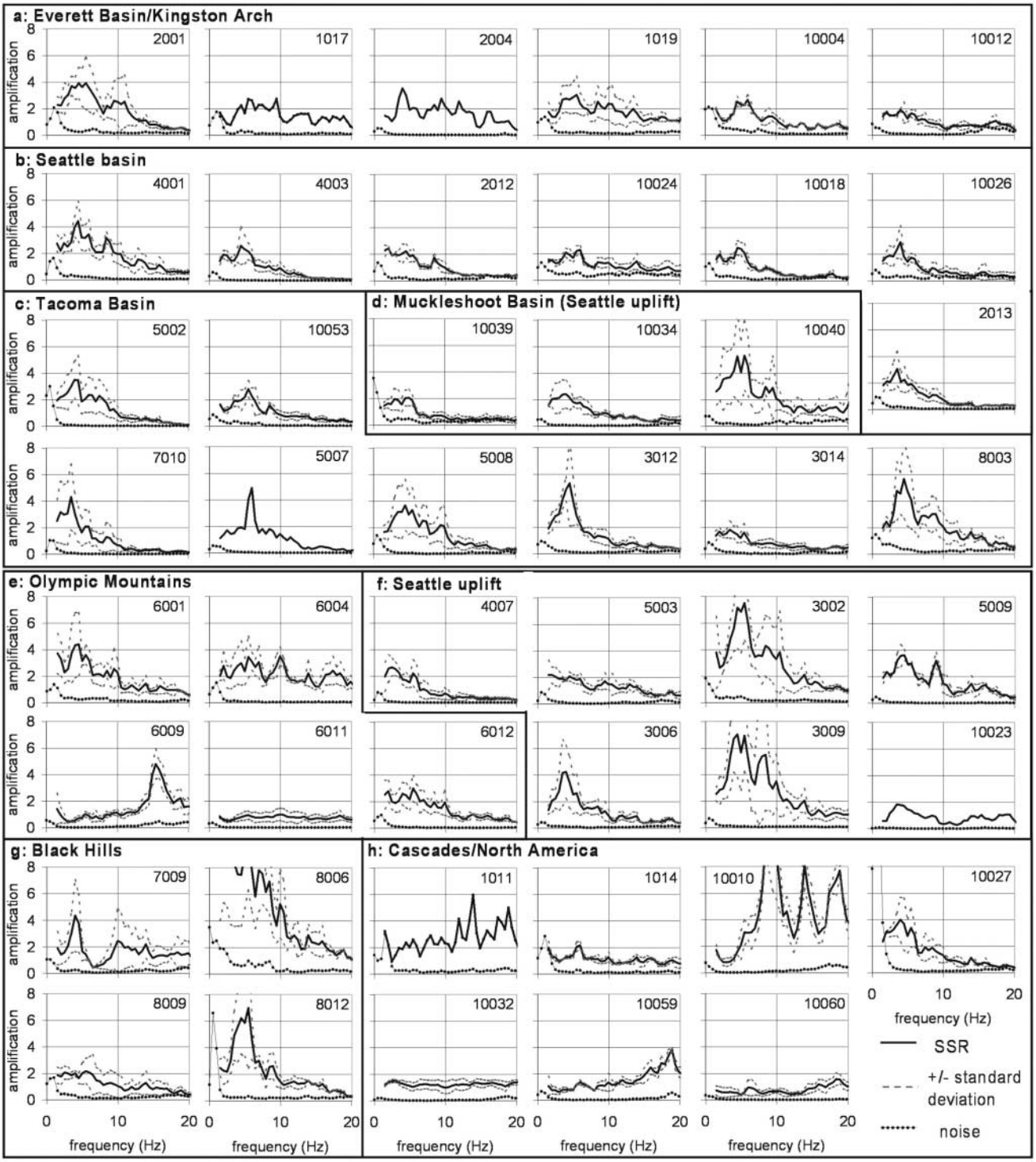

Figure 3. Site-response spectra computed for each of our sites from the average of three earthquakes. Sites are grouped by geologic setting, with noise levels denoted by dotted line and one standard deviation in the average denoted by gray dashed lines. a–d show the site response at sites located over the Everett, Seattle, Tacoma, and Muckleshoot sedimentary basins; remaining sites are over areas of thinner sedimentary strata (<2.5 km). Note that all of the site-response curves at basin sites have a similar shape, which consists of a peak at 3–5 Hz and a decrease in amplification at higher frequencies.

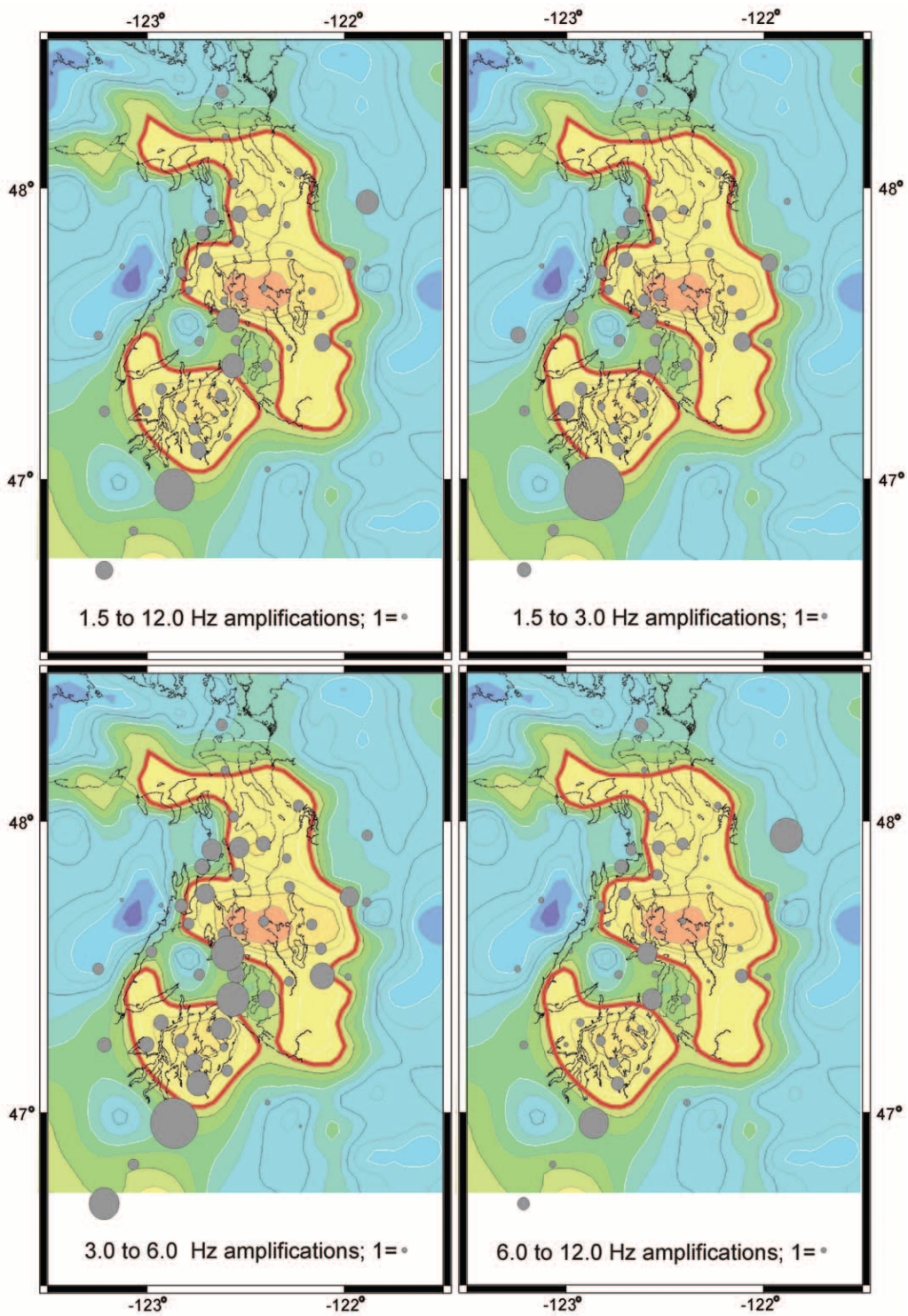

Figure 4. Maps of average SSR amplification superimposed on the tomographic image of *P*-wave velocity at 2.5 km depth. The maps show the average amplification of the SSR values at each site over the four frequency ranges listed at the bottom of each map. An amplitude of 1 is shown in the bottom right of each map. The red lines show the approximate outlines of the Everett, Seattle, and Tacoma sedimentary basins (Fig. 1). Note that the sites over the sedimentary basins show moderate to low amplifications in comparison with some of the surrounding sites.

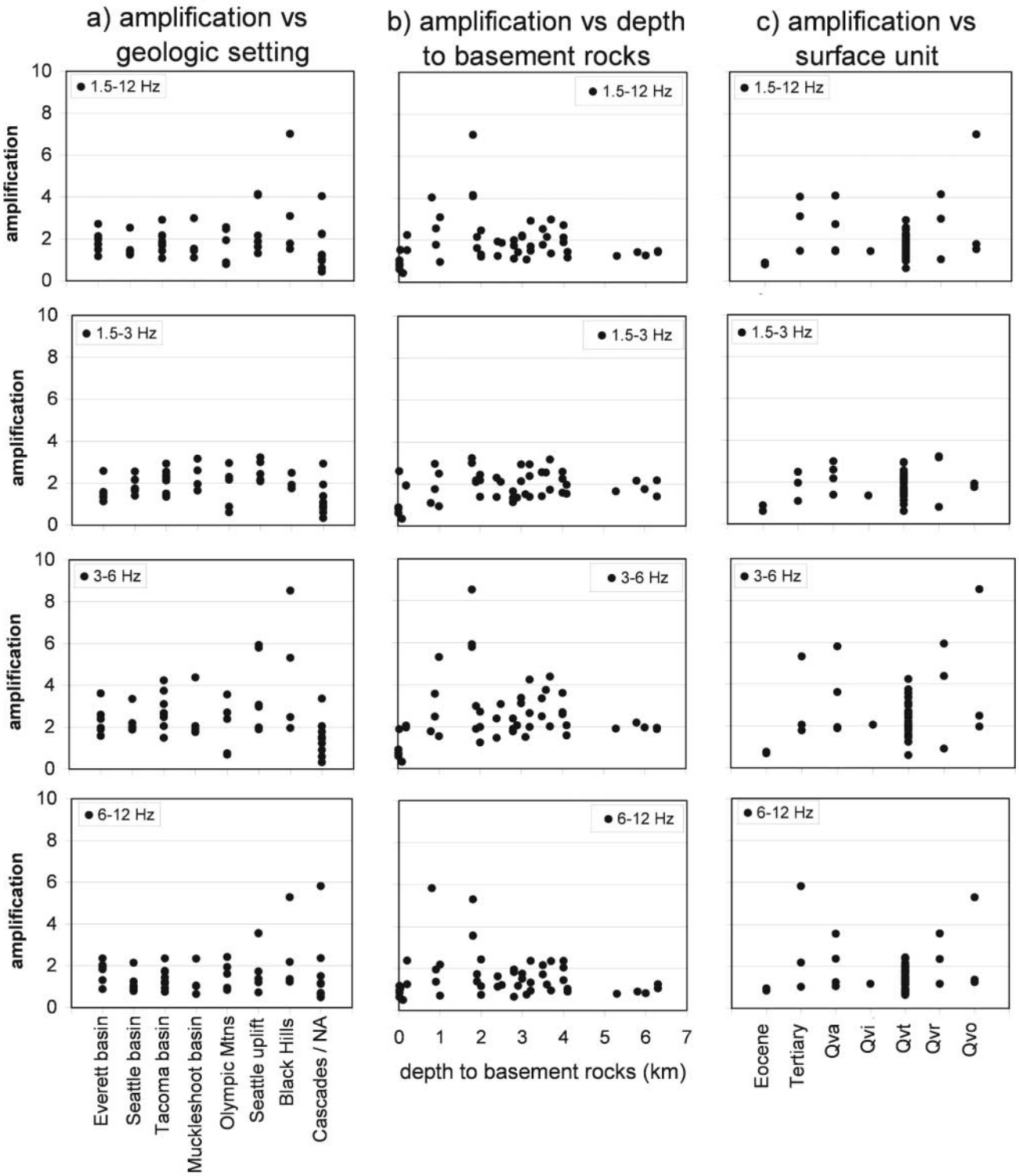

Figure 5. Graphs of spectral amplification (SSR values) versus (a) the geologic setting of each site, (b) the depth to crystalline basement rocks (Crescent Formation, pre-Tertiary North American rocks, or Cascade igneous rocks) below the Tertiary and younger sedimentary strata, and (c) the surface unit at each site. The graphs show the average amplification of the SSR values in the four frequency ranges listed in the top corner of each graph, with each dot representing the average amplification at a receiver site. Qvt, Quaternary Vashon Till; Qva and Qvi, Quaternary advance and interglacial deposits compacted by the thick Vashon ice sheet; Qvo, Quaternary uncompacted glacial outwash; Qvr, Quaternary uncompacted recessional deposits.

frequencies greater than 6 Hz in Figure 5b are consistent with the Seattle basin attenuating seismic energy at frequencies above 7–10 Hz (Pratt *et al.*, 2003). Many sites on the Everett and Tacoma basins show amplifications of less than 1 at frequencies greater than 10 Hz (Fig. 3a,b), indicating significant attenuation of high-frequency seismic waves by all three basins.

The correlation between amplification and mapped surface unit is surprisingly weak (Fig. 5c), although most of the data points are located on one unit (Quaternary Vashon Till [Qvt]). The 1998 SHIPS receivers were situated on Quaternary glacial deposits except for five sites on Eocene volcanic rocks or Tertiary sedimentary rocks, where the seismometers were deployed in a thin (<30 m) layer of sediment on the rock. The Quaternary glacial deposits are subdivided into three general categories: advance and interglacial deposits (Qva, Qvi, Qvt) that were compacted when overridden by the thick Vashon continental ice sheet; uncompacted glacial outwash (Qvo) deposited in front of the glacier; and uncompacted recessional deposits (Qvr) (Galster and Laprade, 1991; Booth, 1994). Because the sites were used for a tomography study, we specifically avoided sites on soft valley fill to ensure we recorded high frequencies and to prevent time delays in the soft sediment. Although sites on Eocene volcanic bedrock show low amplification, there are no consistent and obvious differences in amplification between sites on Tertiary sedimentary rocks, on unconsolidated recessional deposits, and on more compacted advance deposits (Fig. 5c). This lack of correlation may indicate substantial variations in the shallow strata or that the mapped surface units are not representative of the underlying shallow strata.

Comparison of H/V and SSR results

Our H/V results show similar resonance peaks as SSRs at many of our sites, and amplification levels often agree to within a factor of 2, unlike some studies that show large differences in the amplification levels between the H/V and SSR methods (e.g., Riepl *et al.*, 1998; Parolai and Richwalski, 2004). Furthermore, our H/V ratios are larger, in general, than the SSRs at frequencies above the fundamental resonance peak, in contrast to some studies (e.g., Parolai and Richwalski, 2004). This latter observation suggests that our vertical-component amplitudes are relatively weak at basin sites, perhaps because of inefficient mode conversion or relatively few scattered phases and surface waves.

Figure 6 compares our H/V and SSR results, with the H/V shown as a gray line and the SSR as a thin black line. At most of our sites, the H/V spectral ratios have a flatter trend than the SSRs across the frequency spectrum, resulting in many H/V ratios being smaller than SSRs at low frequencies and larger than SSRs at high frequencies (Figs. 6a–h, 7a). This relationship is especially pronounced at basin sites, where the SSRs show low amplitudes above 10 Hz (thin black lines in Figs. 6a–d). The crossover at which SSR values are lower, in general, than the H/V values occurs at about 7–10 Hz (Fig. 6a–h). Both methods identify the main resonance peaks at many sites. For example, prominent resonance peaks at sites 10004 (Fig. 6a), 4001 (Fig. 6b), 5007 (Fig. 6c), 6009 (Fig. 6e), and 5009 (Fig. 6f) have nearly identical shapes using both methods, as do many other peaks. The peaks determined by the two methods clearly do not agree in some cases, however (e.g., 10012, Fig. 6a; 5008, Fig. 6c; 10023, Fig. 6f). At our reference sites, which by definition have SSRs near one, the H/V method gives values about double those given by the SSR method across most of the frequency spectrum (sites 6011 in Fig. 6e and site 10032 in Fig. 6h). Plotting the SSR versus H/V ratios (Fig. 7a) shows that SSRs are consistently larger then the H/V ratios at 2–8 Hz but consistently lower at 8–16 Hz.

To confirm these qualitative observations, we fit a line to the log of the SSR spectral ratios from 2 to 20 Hz to measure their intercepts and slopes (Fig. 8a). The slopes of the SSR trendlines average near zero for sites with shallow bedrock but quickly become negative and lie between 0 and -0.2 for all of our deep basin sites (>2.5 km depth to bedrock; Fig. 8b). These negative slopes indicate decreases in amplification with increasing frequency. At sites where bedrock is less than 2 km deep, the SSR intercepts range from 0 to 9 (with one outlier at 15), but at thick basin sites the intercepts converge toward a value between 2 and 3 (Fig. 8c). For the H/V method, the slopes also begin near 0 at shallow bedrock sites but remain near zero or only slightly negative (0 to -0.1) at nearly all sites (Fig. 8d), confirming the relatively flat responses of the H/V ratios compared with the SSRs. The relatively gentle slopes cause the H/V intercepts (Fig. 8e) to range from 0 to 5 at most sites above shallow bedrock (excluding the outlier), but thick basin sites all have values near 2. Thus, the trendlines demonstrate that the H/V site-response curves consistently show less spectral decay than the SSR curves.

The Effect of Attenuation on Site-Response Curves

We interpret the spectral decay on our SSR curves at sites over thick sedimentary strata as resulting from attenuation, and the slope of the decay should be a measure of the strata's frequency-independent attenuation factor, Q_s (e.g., Anderson and Hough, 1984; Castro *et al.*, 1996; Li *et al.*, 2006). Although we have corrected our spectra for bedrock attenuation, this correction does not take into account the greater attenuation in the sedimentary basins and shallow deposits where shear-wave attenuation factors (Q_s) can be as low as 10 or 20 near the surface and 200 to 300 in deeper basin strata (e.g., Olsen *et al.*, 2003; Li *et al.*, 2006). In our model outlined below we correlate the spectral decay in our SSR response curves with basin thickness and with the thickness of unconsolidated strata. At lower frequencies surface waves that may be independent of total sediment thickness may play a more important role in this analysis than at the higher frequencies analyzed here.

For the H/V site-response curves, the reference signal

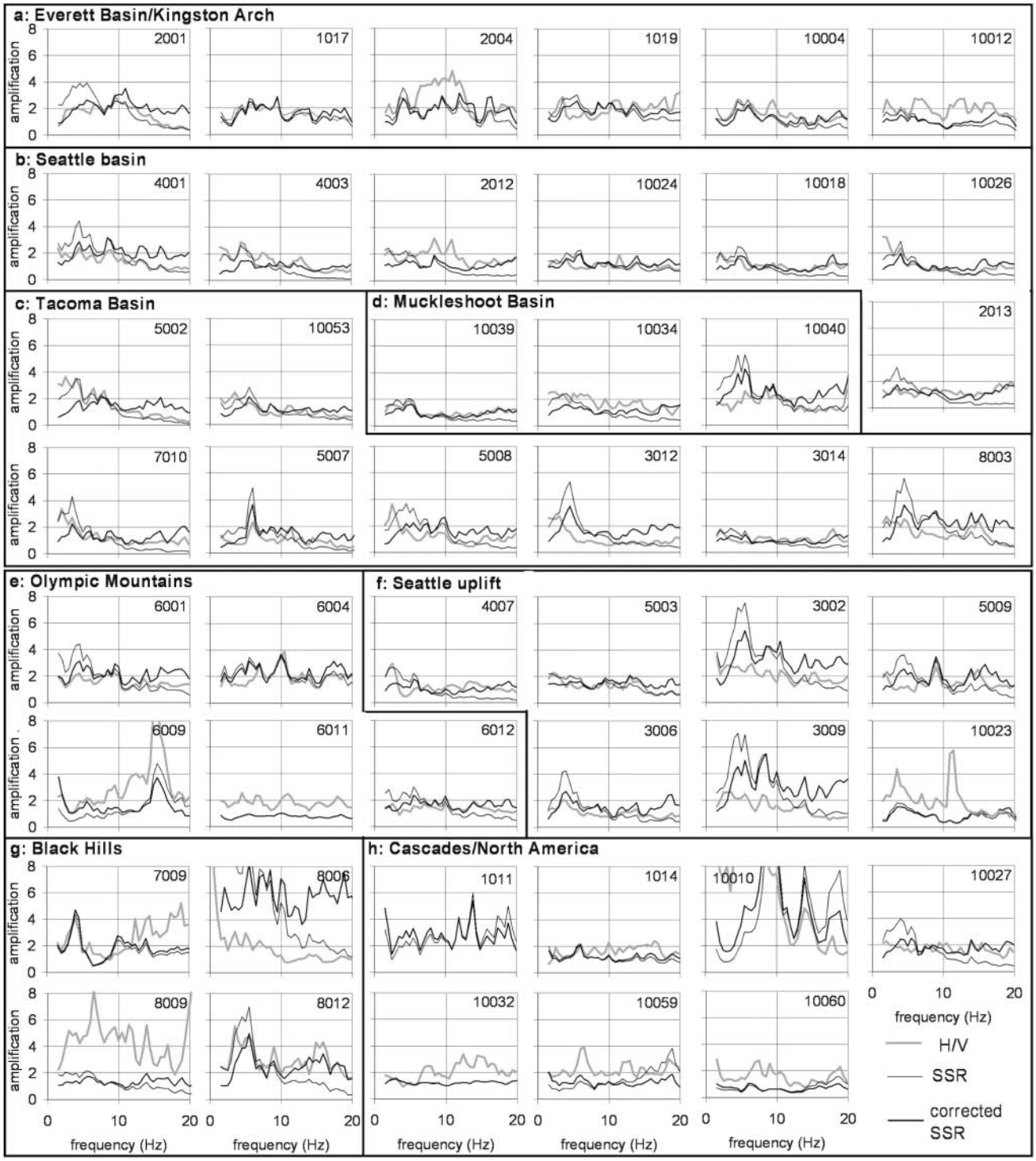

Figure 6. Site responses computed using the SSR method (thin black line) and the H/V method (gray line). The heavy black line shows the SSRs after removing the spectral decay caused by attenuation, as described in the text. After removing the decay, most sites show a closer match between the SSR and H/V values.

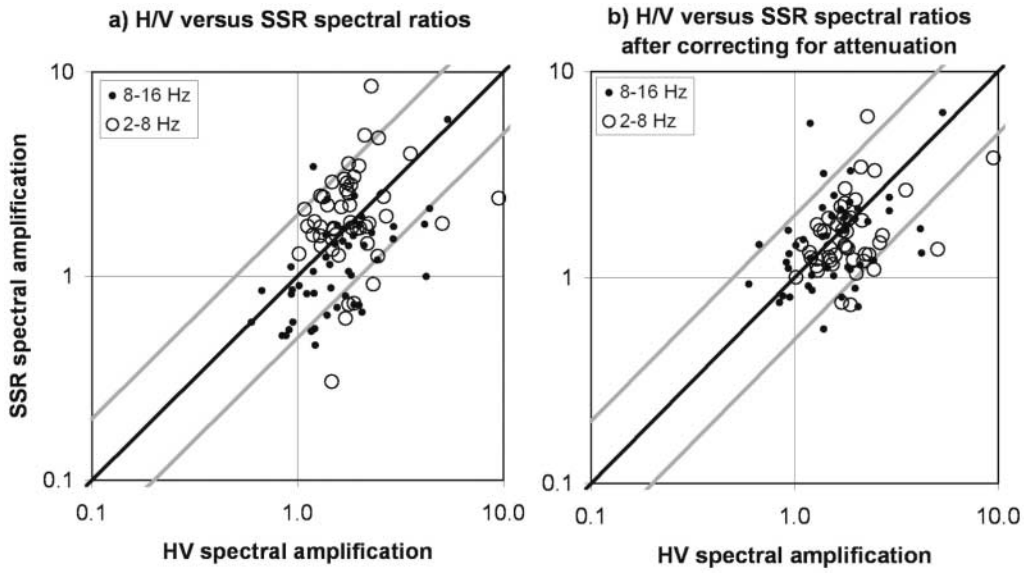

Figure 7. Comparison of SSR and H/V spectral amplifications before (a) and after (b) correcting the SSRs for attenuation. Thick lines show equal values, thin lines show a factor of 2 difference. Before attenuation corrections (a), most of the low-frequency portions have larger SSR values, but at high frequencies the H/V values are larger. After corrections, both high- and low-frequency values show closer agreement between the two methods (b).

(the vertical component) is composed primarily of *S*-to-*P* converted phases and scattered waves originating from *S* waves that have passed through and been attenuated in the basin sediments and shallow deposits. The relatively flat trend of the H/V site-response curves confirms that the reference signal (the vertical component) has undergone attenuation similar to that of the *S* wave recorded on the horizontal components. In contrast, the SSR reference signals recorded at bedrock sites have not undergone attenuation in the basin strata, and the SSRs therefore include the exponential decay caused by greater attenuation at the basin sites. If so, removing the spectral decay from the SSRs should produce a site-response curve that more closely matches the H/V site response.

The shape of the SSR curve at a basin site includes the effects of amplification by low-impedance sedimentary strata, resonance within the sedimentary layers, and attenuation (e.g., Shearer and Orcutt, 1987). Figure 9a, computed using a Thompson-Haskell matrix method (e.g., Aki and Richards, 1980), illustrates the effect of a single layer on the frequency spectrum of a body-wave incident from an underlying half-space. The amplitude spectrum of a seismic wave recorded at the surface will be increased by the bedrock (I_r) to layer (I_l) impedance ratio:

$$A_l/A_r = I_r/I_l = \rho_r v_r/\rho_l v_l, \tag{2}$$

where A = amplitude; ρ = density; v = velocity, and will have a series of amplitude peaks at the fundamental resonant frequency of the layer (f_R) and its higher-order harmonics (Fig. 9a):

$$f_R = (2n + 1)/(2T), \tag{3}$$

where f = frequency, T = two-way travel time through the layer, and $n = 0,1,2 \ldots$ is the resonance mode. At frequencies well below the fundamental resonance peak, where the layer thickness is much smaller than the wavelength, the spectral amplitudes approach the bedrock amplitude of unity (Fig. 9a). Attenuation decreases the size of the higher-order resonance peaks, causing the fundamental peak to be the largest (heavy line in Fig. 9a). When multiple layers are present, the amplitude spectrum at the surface shows a series of resonance peaks caused by the superposition of the resonance peaks from each layer (Fig. 9b). Attenuation again causes the spectral ratio to have a fundamental resonance peak and decreasing spectral amplitudes at higher frequency (Fig. 9b). Adding a deep basin layer further increases the attenuation and steepens the slope of the SSR site response (Fig. 9c), although it is clear from these simple models that most of the attenuation occurs in the shallow strata.

The attenuation of the S waves reaching the surface at basin sites can be described by the equation:

$$A(f) = A_0(f)e^{-\pi f t/Q_s} = A_0(f)e^{-\pi f h/v_s Q_s} = A_0(f)e^{-\pi f t^*}, \tag{4}$$

where $A(f)$ = amplitude at the top of the shallow layers, $A_0(f)$ = amplitude at the base of the sediments, f = frequency, t = travel time, h = sediment thickness (depth to bedrock), v_s = shear-wave velocity in the sediment, and $t^* = h/v_s Q_s$. If we know the thickness of the sedimentary

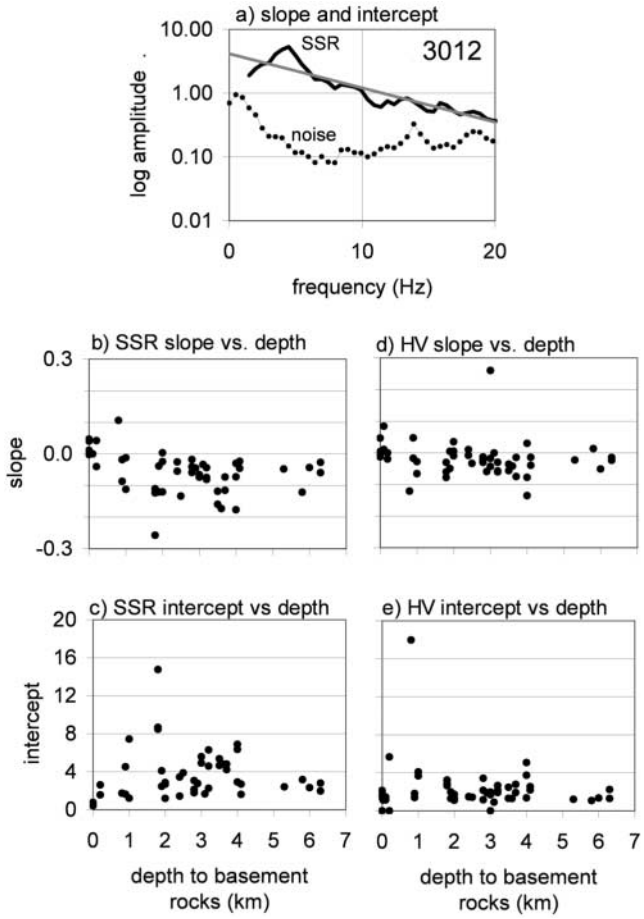

Figure 8. At each site we fit a straight line to the log of the spectral amplification versus frequency (a) and computed the slope and the zero intercept of the slope line. The bottom graphs (b–e) show the slope and intercept values graphed against the depth to basement rocks at each site.

strata and a velocity, the spectral slope of the signal at a site can be used to estimate t^*, or an average, frequency-independent attenuation factor, Q_s, within the underlying basin strata (e.g., Anderson and Hough, 1984; Li *et al.*, 2006). Under the assumption that recordings at the bedrock reference sites do not undergo this attenuation, the slope of the SSR should give an estimate of the attenuation factor (Fig. 9c). Again we emphasize that our high frequencies (>1.5 Hz) are primarily influenced by body waves and scattered phases, but lower frequencies would be influenced more by surface waves (e.g., Joyner, 2000).

The attenuation signatures described previously are evident in the site responses in the Puget Lowland. The SSRs at thick basin sites show an amplification peak at 2–6 Hz and decreasing amplification at higher frequencies, whereas the H/V responses generally have a flatter trend across the 2- to 20-Hz frequency band (Fig. 6a–c). This results in the H/V site responses being smaller at low frequencies, but at frequencies above about 10 Hz the H/V response is almost always larger because attenuation also has decreased the amplitude of the reference signal (Fig. 6a–d). Both methods show many of the same resonance peaks, although clearly not all resonance peaks are common to both methods.

We used equation (4) and the observed spectral decay in the SSRs to estimate an average value for the frequency-independent Q_s for two end-member models for the attenuation. In the first model, we assumed that the attenuation occurs throughout the entire sedimentary column above bedrock. For the second model, we assumed that the attenuation occurs solely within the shallow, unconsolidated deposits. To solve for Q_s using equation (4), we used the average *S*-wave velocity model of the Seattle basin derived from a tomographic analysis of the 1999 SHIPS data by C. Snelson *et al.* (unpublished manuscript, 2006) (Table 3), where depths and velocities are thought to be accurate to within

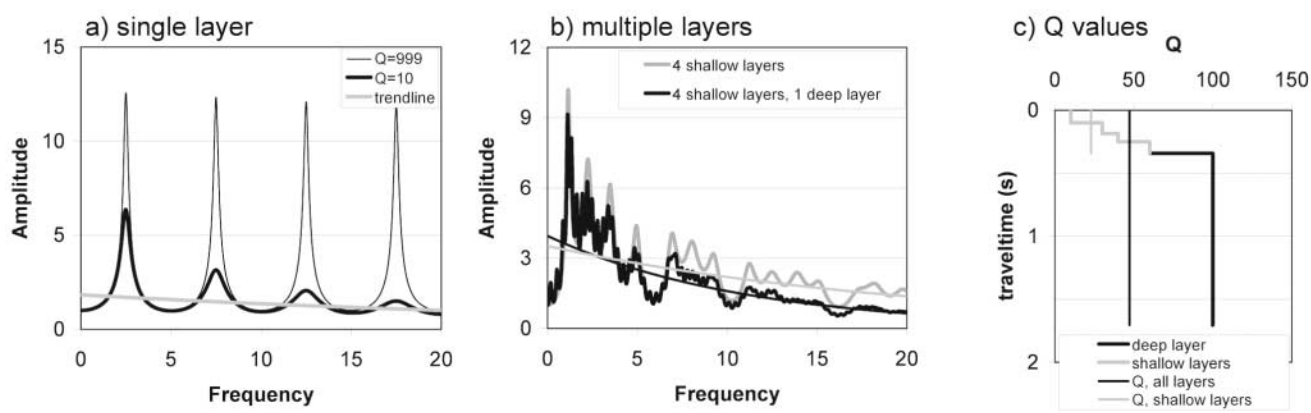

Figure 9. Graph showing the amplitude response of a single, shallow layer without and with attenuation (a), and the same graphs for a four-layer model representative of sedimentary strata with and without a deeper layer (b). Graph (c) shows the comparison of values of Q in the input models with those obtained from the trend of the amplitude decrease at higher frequencies. Graphs were computed using a Thompson-Haskell matrix method (Aki and Richards, 1980).

about 10%. In equation (4) we have also used the depth to bedrock and thickness of unconsolidated deposits beneath each site (Table 1). In the basin model, we removed the original bedrock attenuation correction (equation 1) for a distance equal to the basin thickness so that the spectral decay correctly measures the attenuation in the sediment portion of the raypath. We ignored this correction for model 2 because the unconsolidated deposits are thin (< 1.1 km). We computed error bars by using the 95% confidence value for the slope, and a 20% estimated error in the thickness of sedimentary strata and unconsolidated strata. This latter uncertainty may sound large, but there are few drill-hole data in much of the area and estimates of the Seattle basin thickness range from 7.5 km (Pratt *et al.*, 1997) to 10 km (Brocher *et al.*, 2001).

We plot the resulting values for Q_s at our sites against total basin thickness and against thicknesses of unconsolidated sediments in Figure 10. These plots do not include the nonbasin sites with a negative spectral slope. Plotted against depth to bedrock, the values form two groups: a cluster of lower values that contains most of the points, and outliers with high Q_s values. As depth to bedrock increases, the average Q_s within the overlying strata increases, presumably reflecting the contribution of the consolidated, less attenuating sedimentary rocks deeper in the basin. There is also an unknown contribution from scattered phases that may or may not correlate directly with basin thickness. Most Q_s values lie between 30 and 100, but these average values are time-weighted toward the low-velocity, shallow strata. Plotted against the thickness of unconsolidated deposits, there is a clear trend of increasing Q_s with increasing deposit thickness, with less scatter than for Q_s versus total basin thickness. The reduced scatter in Figure 10b suggests that most of the attenuation indeed occurs within the unconsolidated deposits, and that the total basin thickness is less important to determining the attenuation of these high-frequency signals.

We inverted for depth-averaged Q_s values to see if they match independently obtained values for the Seattle basin (Li *et al.*, 2006). We assumed an exponential increase in Q_s with depth, and fit a curve through the data points of the form:

$$Q_s = a + bz^c, \tag{5}$$

where z is the depth to bedrock in kilometers, and a, b, and c are variables (Fig. 10a,b). This equation was chosen because it allows for a steady increase in Q_s values when we invert for Q_s versus depth (see below). We also bracket the clusters of points using higher and lower values in equation (5) (Fig. 10a,b; Table 4). Because this function depends primarily on the stratal thickness, it does not properly account for scattered phases that do not correlate with thicker sections of unconsolidated strata.

We inverted equation (5) for $1/Q_{s,\mathrm{int}}$ (intrinsic attenuation in a depth interval) for layers 0.2 km thick at the surface

Table 3
Seattle Basin *S*-Wave Velocity Function
(Snelson *et al.*, unpublished work)

Depth (km)	Velocity (km/sec)
0	0.5
4	1.3
6	2.4
9	3.4
15	4.0

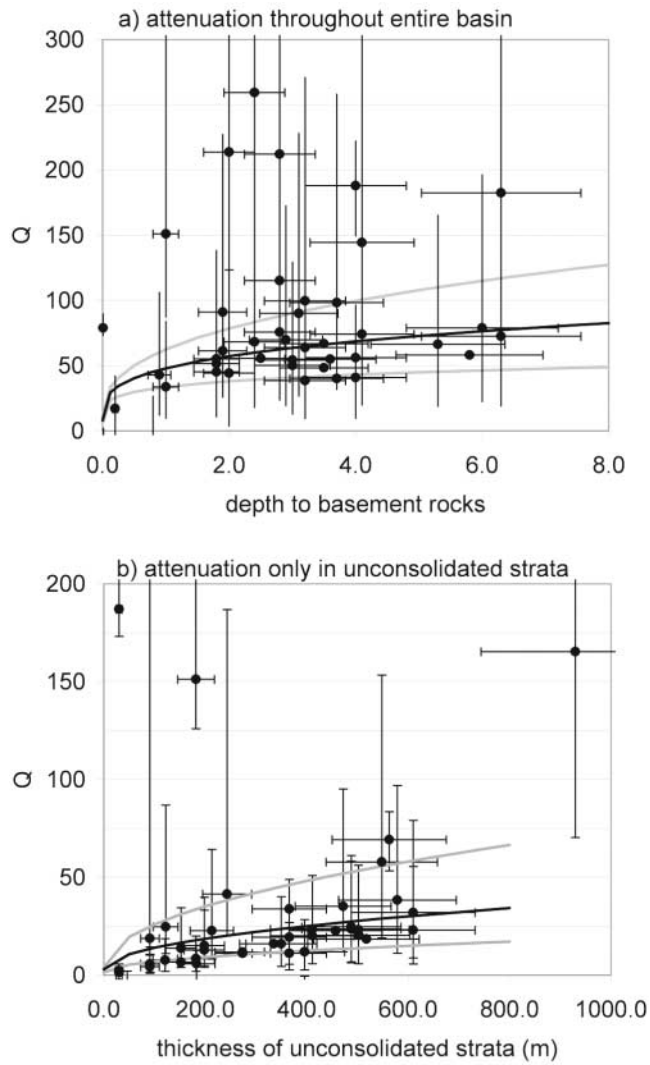

Figure 10. Attenuation factors (Q_s) derived from the slope of the log of the SSR (equation 4) (Fig. 6a) plotted against the depth to top of basement rocks (in kilometers): (a) assuming that attenuation is distributed throughout the entire thickness of sedimentary strata, (b) assuming attenuation occurs entirely within the unconsolidated deposits. Error bars are computed from the 95% confidence of the slope regression (Fig. 8a) and assuming a 20% error in the depth determinations. Dark line is the preferred Q-versus-depth function, gray lines are upper and lower bounds computed using equation (5) and the values listed in Table 4.

and increasing to 0.5 km thick. For the unconsolidated deposits we used 25-m-thick layers. This inversion was done using the travel time to the top and bottom of the layer (t_i and t_{i+1}) and the average Q at the top and bottom of the layer from equation (4) (Q_i and Q_{i+1}):

$$Q_{s,\mathrm{int}} = (t_{i+1} - t_i)/(t_{i+1}/Q_{i+1} - t_i/Q_i).$$

Our results for the entire basin thickness show $Q_{s,\mathrm{int}}$ values of less than 40 near the surface, increasing to about 250 in the deepest sedimentary rocks (Fig. 11a). The shape of the curve mimics the velocity function (Table 3) on which the inversion depends. The high and low bounds result in interval $Q_{s,\mathrm{int}}$ values ranging from 90 to greater than 1000 in the deeper basin strata. These values are broadly consistent with an inversion for Q_s in the Seattle basin carried out by Li *et al.* (2006) (Fig. 11a) using data recorded in the 1999 SHIPS experiment (Brocher *et al.*, 2000b). Li *et al.* (2006) computed values of 16 to 160 (1 and 8 Hz) at the top of the basin and 40 to 300 (1 and 8 Hz) at about 8 km depth.

For the model in which all of the attenuation occurs in the unconsolidated deposits (Fig. 10b), the $Q_{s,\mathrm{int}}$ values are lower, as expected. For this model, the $Q_{s,\mathrm{int}}$ values are 5 to 20 at the surface and increase to 40 to 160 at 0.9 km depth (Fig. 11b).

Our depth-averaged Q_s values are only loosely constrained (Fig. 10); however, equation (5) satisfies most of the data points and our $Q_{s,\mathrm{int}}$ inversion for the entire basin thickness yields reasonable values comparable with other studies (Li *et al.*, 2006). This agreement indicates that the observed spectral decay in the SSRs can be satisfactorily explained at most sites by attenuation within the sedimentary strata.

Correcting SSRs for Attenuation

If our SSRs include the effects of attenuation whereas our H/V ratios do not, removing the spectral decay from the SSRs should bring them into better agreement with the H/V ratios. To test this hypothesis, we divided each of the SSRs by its best-fitting attenuation curve (equation 4) (Fig. 8a). This division removes the overall spectral decay (flattens the SSR curve), resulting in a spectral ratio with an average value

Table 4
Values Used in Equation (5)

Attenuation	a	b	c
Through entire basin			
Low	5.6	28	0.21
Center	8	40	0.3
High	10.4	52	0.39
Within unconsolidated strata			
Low	1.5	17.5	0.5
Center	3	35	0.5
High	3.9	70	0.5

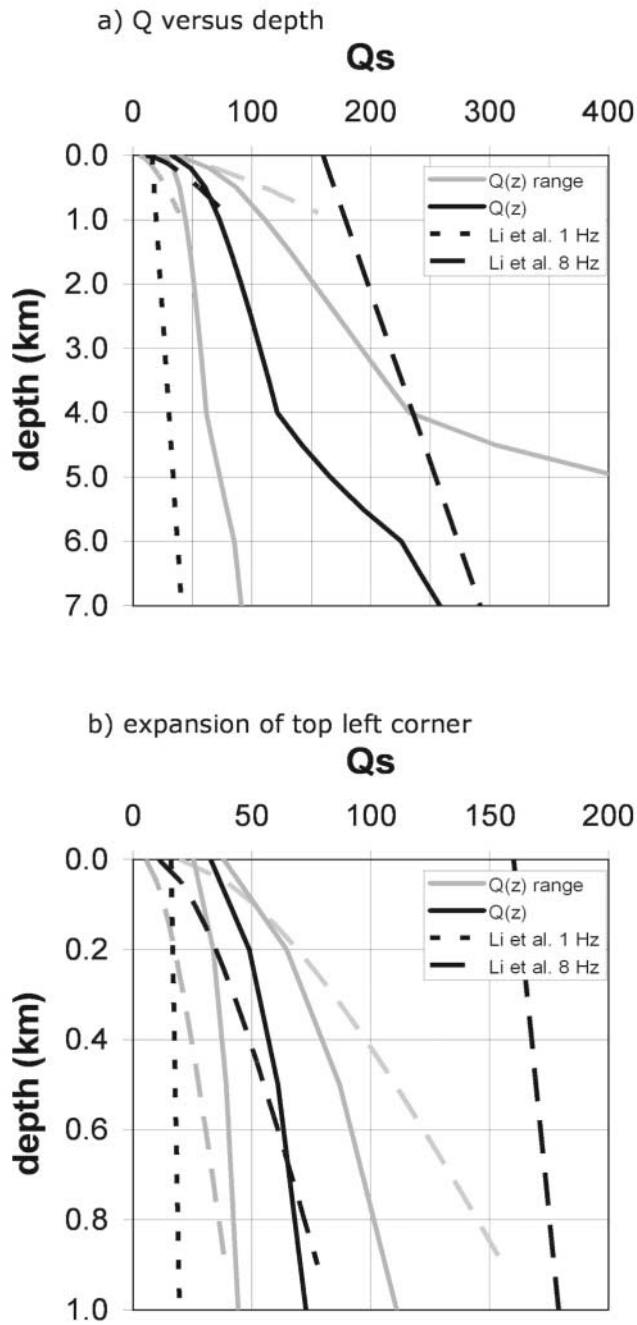

Figure 11. (a) Values of Q in each depth interval $Q_{s,\mathrm{int}}$ derived from inversion of the average Q_s (Fig. 10). Solid lines assume attenuation distributed throughout the entire basin, dashed lines assume attenuation occurs only in the unconsolidated deposits. Black lines show preferred model, gray lines show upper and lower bounds (Fig. 10). (b) Bottom graph shows an expansion of the top left corner of the upper graph. For the basin model, values of interval $Q_{s,\mathrm{int}}$ increase from 25 to 20 in the near surface to a range of 100 to over 1000 at 7 km depth. For attenuation only in the unconsolidated strata, $Q_{s,\mathrm{int}}$ ranges from 5 to 20 at the surface to values of 40 to 160 at 0.9 km depth. Our results lie within the range of the inversion results Li *et al.* (2006) for the Seattle Basin between 1 and 8 Hz.

of 1, but retains the resonance peaks. For sites that have a relatively flat trend, the process has little effect on the shape. The corrected curves need to be scaled to obtain the overall amplification factor. In principle this scaling could be computed from the intercept value (A_0), but this value is strongly influenced by the fundamental frequency and amplification of the dominant resonance peak. We therefore took the alternative approach of scaling the attenuation-corrected SSR values by the average amplification of the uncorrected SSR curve. This ensures that the original and corrected SSRs have the same average amplification. In practice, we found a close fit when we scaled the attenuation-corrected SSR values to the average of the initial SSR values in the 2- to 16-Hz frequency range.

In many cases, the attenuation-corrected SSRs are in closer agreement with the H/V ratios than are the uncorrected SSRs (Figs. 6a–h). When we compare the average values in the 2- to 8-Hz and 8- to 16-Hz frequency ranges, we find that most (84%) of the attenuation-corrected SSRs match the H/V amplifications within a factor of 2 (Fig. 7b). In particular, the systematic differences between low and high frequencies have been removed, and average values in both frequency ranges are nearly equivalent between the two methods (Fig. 7b).

Discussion and Conclusions

Our SSRs show that although the major sedimentary basins beneath the Puget Lowland substantially amplify seismic waves at frequencies below 7–10 Hz, their strata have a net attenuating effect on seismic waves at frequencies higher than 7–10 Hz. Our results are consistent with those of Pratt *et al.* (2003), who also reported amplification of weak ground motions over the Seattle basin at frequencies below 7 Hz and attenuation at higher frequencies. Our data indicate that the Tacoma and Everett basins show a similar pattern.

The SSR results show larger site amplifications over the Tacoma basin than the Seattle and Everett basins to the north (Fig. 3a–c). We speculate that the cause of the southward increase in SSR amplification levels in these basins is that the glacial deposits are less compacted to the south because the area was overridden by southward thinning ice during the last major glacial advance (Booth, 1994; Thorson, 1980, 1996). Measurements of soil compaction indicate a correlation with ice thickness (e.g., LaPrade, 1982), indicating that a southward thinning glacier will cause a southward decrease in compaction. Consistent with this inference, shallow velocity measurements indicate a southward decrease of *P*-wave velocities in the shallow sediments (K. Ramachandran, unpublished manuscript, 2006). This evidence suggests that the ice sheet exerts control on the site response in the region. Alternative explanations are that the glacial deposits could change thickness or character at the south end of the Puget Lowland. The suggestion that the amount of attenuation within the basement rocks decreases to the south is less likely, given that Crescent Formation volcanic rocks underlie both the southern and central Puget Lowland region.

Nonbasin sites exhibit a wider variety of shapes to the site responses than do the thick basin sites, with a depth to the top of bedrock of about 2 km defining the transition from variable site response to the more consistent basin response (Fig. 5b). We speculate that this variation in site response reflects the influence of irregularities in the bedrock surface and a greater variety of stratification in areas of shallow bedrock. As bedrock deepens, its influence on the site response from three-dimensional effects such as focusing is diminished by the more uniform response of the relatively flat sedimentary strata.

Site responses over thick sedimentary basins in the Puget Lowland demonstrate that attenuation in the basins causes systematic differences between SSR and H/V site-response estimates. Because the reference signal used in the H/V method (the vertical component recordings of the shear waves) has undergone attenuation similar to the horizontal component recordings, the H/V method shows lower amplification than SSRs at low frequencies and does not show as much decrease in amplification with increasing frequency. These differences are consistent with *S*-to-*P* mode conversion at shallow levels in the sedimentary section after undergoing *S*-wave attenuation in the deeper strata.

Using the spectral decay in the SSR amplification curves to estimate the attenuation in the basins results in interval $Q_{s,\mathrm{int}}$ values of less than 40 in the near-surface sediments, increasing to about 250 at the bottom of the basins. Although these estimates pertain to the Everett, Seattle, and the Tacoma basins, these values agree with an independent estimate from the Seattle basin (Li *et al.*, 2006), and from estimates of Q_s in other Cenozoic basins (summary in Olsen *et al.*, 2003).

Correcting the SSRs for attenuation within the basins beneath the Puget Lowland improved the match with the H/V estimates. After attenuation corrections, the SSR method shows many of the same resonance peaks as the H/V method. This similarity implies that the SSRs consist of the shallow resonance and other impedance effects (the H/V site response) superimposed on a spectral decay curve. The H/V method appears to identify the predominant resonance peaks caused by shallow strata beneath many sites, as concluded from examination of data from borehole seismometers (e.g., Tsuboi *et al.*, 2001). Whereas SSRs contain the full site response and attenuation effects, H/V site responses primarily reflect the resonance and amplification effects of the shallow sediments. H/V responses therefore can be predicted from SSR responses, but SSR responses cannot be predicted from H/V responses without independent estimates of attenuation within the basin strata.

Acknowledgments

We thank the many volunteers and staff who deployed and maintained the SHIPS seismometers, and the landowners for allowing us to install in-

struments on their property. Derek Booth and Ralph Haugerud provided the geologic information, Robert Crosson provided the tomography images, and Cathy Snelson provided the velocity model. Amy Wright of the Pacific Northwest Seismic Network computed the focal mechanisms. The seismographs were provided by the Program for Array Seismic Studies of the Continental Lithosphere (PASSCAL) of the Incorporated Research Institutes for Seismology (IRIS). The manuscript has benefited by reviews from Steve Hartzell, Joe Fletcher, and two anonymous reviewers.

References

Aki, K., and P. G. Richards (1980). *Quantitative Seismology: Theory and Methods*, W. H. Freeman and Co., San Francisco, 932 pp.

Anderson, J. G., and S. E. Hough (1984). A model for the shape of the Fourier amplitude spectrum of acceleration at high frequencies, *Bull. Seism. Soc. Am.* **74,** 1969–1993.

Atkinson, G. M. (1995). Attenuation and source parameters of earthquakes in the Cascadia region, *Bull. Seism. Soc. Am.* **85,** 1327–1342.

Barberopoulou, A., A. Qamar, T. L. Pratt, K. C. Creager, and W. P. Steele (2004). Local amplification of seismic waves from the Mw7.9 Alaska earthquake and damaging water waves in Lake Union, Seattle, Washington, *Geophys. Res. Lett.* **31,** L03607, doi 10.1029/2003GL018569.

Bonilla, L. F., J. H. Steidl, G. T. Lindley, A. G. Tumarkin, and R. J. Archuleta (1997). Site amplification in the San Fernando valley, California: variability of site-effect estimation using the S-wave, Coda, and H/V methods, *Bull. Seism. Soc. Am.* **87,** 710–730.

Booth, D. B. (1994). Glaciofluvial infilling and scour of the Puget Lowland, Washington, during ice-sheet glaciation, *Geology* **22,** 695–698.

Brocher, T. M., R. J. Blakely, and R. E. Wells (2004). Interpretation of the Seattle uplift, Washington, as a passive roof duplex, *Bull. Seism. Soc. Am.* **94,** 1379–1401.

Brocher, T. M., T. Parsons, R. J. Blakely, N. I. Christensen, M. A. Fisher, and R. E. Wells, and SHIPS Working Group (2001). Upper crustal structure in Puget Lowland, Washington: Results from the 1998 Seismic Hazards Investigation in Puget Sound, *J. Geophys. Res.* **106,** 13,541–13,564.

Brocher, T. M., T. Parsons, K. C. Creager, R. S. Crosson, N. P. Symons, G. D. Spence, B. C. Zelt, P. T. C. Hammer, R. D. Hyndman, D. C. Mosher, A. M. Tréhu, K. C. Miller, M. A. Fisher, T. L. Pratt, M. G. Alvarez, B. C. Beaudoin, K. E. Louden, and C. S. Weaver (1999). Wide-angle seismic recordings from the 1998 seismic hazards investigation of Puget Sound (SHIPS), western Washington and British Columbia, *U.S. Geol. Surv. Open-File Rept. 99-314*, 110 pp. http://geopubs.wr.usgs.gov/open-file/of99-314/.

Brocher, T. M., T. L. Pratt, K. C. Creager, R. S. Crosson, W. P. Steele, C. S. Weaver, A. D. Frankel, A. M. Tréhu, C. M. Snelson, K. C. Miller, S. H. Harder, and U. S. ten Brink (2000a). Urban seismic experiments investigate Seattle fault and basin, *Eos*, *Trans. AGU* **81,** 545, 551–552.

Brocher, T. M., T. L. Pratt, K. C. Miller, A. M. Tréhu, C. M. Snelson, C. S. Weaver, K. C. Creager, R. S. Crosson, U. S. ten Brink, M. G. Alvarez, S. H. Harder, and I. Asudeh (2000b). Report for explosion and earthquake data acquired in the 1999 Seismic Hazards Investigation in Puget Sound (SHIPS), Washington, *U.S. Geol. Surv. Open-File Rept. 00-318*, 85 pp. http://geopubs.wr.usgs.gov/open-file/of00-318/.

Castro, R. R., M. Mucciarelli, F. Pacor, and C. Petrungaro (1997). S-wave site-response estimates using horizontal-to-vertical spectral ratios, *Bull. Seism. Soc. Am.* **87,** 256–260.

Castro, R. R., F. Pacor, A. Sala, and C. Petrungaro (1996). S wave attenuation and site effects in the region of Friuli, Italy, *J. Geophys. Res.* **101,** 22,355–22,369.

Dutta, U., A Martirosyan, N. Biswas, A. Papageorgiou, and R. Combellick (2001). Estimation of S-wave site response in Anchorage, Alaska, from weak-motion data using generalized inversion method, *Bull. Seism. Soc. Am.* **91,** 335–346.

Field, E. H., and K. H. Jacob (1995). A comparison and test of various site-response estimation techniques, including three that are not reference-site dependent, *Bull. Seism. Soc. Am.* **85,** 1127–1143.

Fisher, M. A., T. M. Brocher, R. D. Hyndman, A. M. Tréhu, C. S. Weaver, K. C. Creager, R. S. Crosson, T. Parsons, A. K. Cooper, D. Mosher, G. Spence, B. C. Zelt, P. T. Hammer, U. S. ten Brink, T. L. Pratt, K. C. Miller, J. R. Childs, G. R. Cochrane, S. Chopra, and R. Walia (1999). Seismic survey probes urban earthquake hazards in Pacific Northwest, *Eos*, *Trans. AGU* **80,** no. 2, 13–17.

Frankel, A. (1994). Dense array recordings in the San Bernardino Valley of Landers–Big Bear aftershocks: Basin surface waves, Moho reflections, and three-dimensional simulations, *Bull. Seism. Soc. Am.* **84,** 613–624.

Frankel, A., D. Carver, E. Cranswick, M. Meremonte, T. Bice, and D. Overturf (1999). Site response for Seattle and source parameters of earthquakes in the Puget Sound region, *Bull. Seism. Soc. Am.* **89,** 468–483.

Frankel, A. D., D. L. Carver, and R. A. Williams (2003). Nonlinear and linear site response and basin effects in Seattle for the M6.8 Nisqually, Washington, earthquake, *Bull. Seism. Soc. Am.* **92,** 2090–2109.

Galster, R. W., and W. T. Laprade (1991). Geology of Seattle, Washington, United States of America, *Bull. Assoc. Eng. Geol.* **28,** 235–302.

Hartzell, S. (1992). Site response estimation from earthquake data, *Bull. Seism. Soc. Am.* **82,** 2308–2327.

Hartzell, S., D. Carver, E. Cranswick, and A. Frankel (2000). Variability of site response in Seattle, Washington, *Bull. Seism. Soc. Am.* **90,** 1237–1250.

Hartzell, S., A. Leeds, A. Frankel, and J. Michael (1996). Site response for urban Los Angeles using aftershocks of the Northridge earthquake, *Bull. Seism. Soc. Am.* **86,** S168–S192.

Johnson, S. Y., C. J. Potter, and J. M. Armentrout (1994). Origin and evolution of the Seattle fault and Seattle basin, Washington, *Geology* **22,** 71–74.

Johnson, S. Y., C. J. Potter, J. M. Armentrout, J. J. Miller, C. Finn, and C. S. Weaver (1996). The southern Whidbey Island fault: An active structure in the Puget Lowland, Washington, *Geol. Soc. Am. Bull.* **108,** 334–354.

Jones, M. A. (1996). Thickness of unconsolidated deposits in the Puget Sound Lowland, Washington and British Columbia, *U.S. Geol. Surv. Water Res. Invest. Rept. 94-4133*, 1 plate, scale 1:454,545.

Joyner, W. B. (2000). Strong motion from surface waves in deep sedimentary basins, *Bull. Seism. Soc. Am.* **90,** S95–S112.

LaPrade, W. T. (1982). Geologic implications of pre-consolidated pressure values, Lawton clay, Seattle, Washington, in *Proc. of the 19th Annual Engineering Geology and Soils Engineering Symposium*, Idaho State University, Pocatello, Idaho, 303–321.

Lermo, J., and F. J. Chávez-Garcia (1993). Site effect evaluation using spectral ratios with only one station, *Bull. Seism. Soc. Am.* **83,** 1574–1594.

Li, Q., W. S. D. Wilcock, T. L. Pratt, C. M. Snelson, and T. M. Brocher (2006). Seismic attenuation structure of the Seattle basin, Washington State, from explosive-source refraction data, *Bull. Seism. Soc. Am.* **96,** no. 2, 553–571.

Liu, H.-L., and T. Heaton (1984). Array analysis of the ground velocities and accelerations from the 1971 San Fernando, California, earthquake, *Bull. Seism. Soc. Am.* **74,** 1951–1968.

Martirosyan, A., U. Dutta, N. Biswas, A. Papageorgiou, and R. Combellick (2002). Determination of site response in Anchorage, Alaska, on the basis of spectral ratio methods, *Earthquake Spectra* **18,** 85–104.

Olsen, K. B., S. M. Day, and C. R. Bradley (2003). Estimation of Q for long-period (>2 sec) waves in the Los Angeles basin, *Bull. Seism. Soc. Am.* **93,** 627–638.

Parolai, S., and S. M. Richwalski (2004). The importance of converted waves in comparing H/V and RSM site response estimates, *Bull. Seism. Soc. Am.* **94,** 304–313.

Pratt, T. L., T. M. Brocher, C. S. Weaver, K. C. Miller, A. M. Tréhu, K. C. Creager, and R. S. Crosson (2003). Amplification of seismic waves

by the Seattle basin, Washington State, *Bull. Seism. Soc. Am.* **93,** 533–545.

Pratt, T. L., S. Johnson, C. Potter, W. Stephenson, and C. Finn (1997). Seismic reflection images beneath Puget Sound, western Washington State: the Puget lowland thrust sheet hypothesis, *J. Geophys. Res.* **102,** 27,469–27,489.

Riepl, J., P.-Y. Bard, D. Hatzfeld, C. Papaioannou, and S. Nechtschein (1998). Detailed evaluation of site-response estimation methods across and along the sedimentary valley of Volvi (EURO-SEISTEST), *Bull. Seism. Soc. Am.* **88,** 488–502.

Sánches-Sesma, F. J., S. Chávez-Pérez, M. Suarez, M. A. Bravo, and L. E. Pérez-Rocha (1988). On the seismic response of the Valley of Mexico, *Earthquake Spectra* **4,** 569–589.

Sánches-Sesma, F. J., L. E. Pérez-Rocha, and E. Reinoso (1993). Ground motion in Mexico City during the April 25, 1989, Guerrero earthquake, *Tectonophysics* **218,** 127–140.

Satoh, T., H. Kawase, and S. Matsushima (2001). Differences between site characteristics obtained from microtremors, S-waves, P-waves and codas, *Bull. Seism. Soc. Am.* **91,** 313–334.

Shearer, P. M., and J. A. Orcutt (1987). Surface and near-surface effects on seismic waves—theory and borehole seismometer results, *Bull. Seism. Soc. Am.* **77,** 1168–1196.

Thorson, R. M. (1980). Ice-sheet glaciation of the Puget Lowland, Washington, during the Vashon Stade (late Pleistocene), *Quat. Res.* **13,** 303–321.

Thorson, R. M. (1996). Earthquake recurrence and glacial loading in western Washington, *Geol. Soc. Am. Bull.* **108,** 1182–1191.

Tsuboi, S., M. Saito, and Y. Ishihara (2001). Verification of horizontal-to-vertical spectral-ratio technique for estimation of site response using borehole seismographs, *Bull. Seism. Soc. Am.* **91,** 499–510.

Van Wagoner, T. M., R. S. Crosson, K. C. Creager, G. Medema, L. Preston, N. P. Symons, and T.M. Brocher (2002). Crustal structure and relocated earthquakes in the Puget Lowland, Washington from high resolution seismic tomography, *J. Geophys. Res.* **107,** B12, ESE 22-1–ESE 22-23, doi 10.10129/2001JB000710.

Wald, D. J., and R. W. Graves (1998). The seismic response of the Los Angeles Basin, California, *Bull. Seism. Soc. Am.* **88,** 337–356.

Williams, R. A., W. J. Stephenson, A. D. Frankel, E. Cranswick, M. E. Meremonte, and J. K. Odum (2000). Correlation of 1- to 10-Hz earthquake resonances with surface measurements of P- and S-wave reflections and refractions in the upper 50 m, *Bull. Seism. Soc. Am.* **90,** 1323–1331.

Williams, R. A., W. J. Stephenson, A. D. Frankel, and J. K. Odum (1999). Surface seismic measurements of near-surface P- and S-wave seismic velocities at earthquake recording stations, Seattle, Washington, *Earthquake Spectra* **15,** 565–584.

Yu, G., and J. Haines (2003). The choice of reference sites for seismic ground amplification analyses: case study at Parkway, New Zealand, *Bull. Seism. Soc. Am.* **93,** 713–723.

U.S. Geological Survey
School of Oceanography
Box 357940
University of Washington
Seattle, Washington 98195
(T.L.P.)

U.S. Geological Survey
MS 977, 345 Middlefield Road
Menlo Park, California 94025
(T.M.B.)

Manuscript received 22 October 2004.